

pubs.acs.org/accounts Article

Exploring Gas-Liquid Reactions with Microjets: Lessons We Are Learning

Published as part of the Accounts of Chemical Research special issue "Applications of Liquid Microjets in Chemistry".

Xiao-Fei Gao and Gilbert M. Nathanson*



Cite This: https://doi.org/10.1021/acs.accounts.2c00602

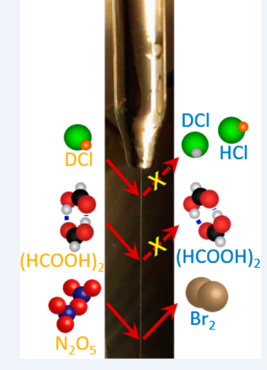


ACCESS

Metrics & More

Article Recommendations

CONSPECTUS: Liquid water is all around us: at the beach, in a cloud, from a faucet, inside a spray tower, covering our lungs. It is fascinating to imagine what happens to a reactive gas molecule as it approaches the surface of water in these examples. Some incoming molecules may first be deflected away after colliding with an evaporating water molecule. Those that do strike surface H_2O or other surface species may bounce directly off or become momentarily trapped through hydrogen bonding or other attractive forces. The adsorbed gas molecule can then desorb immediately or instead dissolve, passing through the interfacial region and into the bulk, perhaps diffusing back to the surface and evaporating before reacting. Alternatively, it may react with solute or water molecules in the interfacial or bulk regions, and a reaction intermediate or the final product may then desorb into the gas phase. Building a "blow by blow" picture of these pathways is challenging for vacuum-based techniques because of the high vapor pressure of water. In particular, collisions within the thick vapor cloud created by evaporating molecules just above the surface scramble the trajectories and internal states of the gaseous target molecules, hindering construction of gas—liquid reaction mechanisms at the atomic scale that we strive to map out.



The introduction of the microjet in 1988 by Faubel, Schlemmer, and Toennies opened up entirely new

possibilities. Their inspired solution seems so simple: narrow the end of a glass tube to a diameter smaller than the mean free path of the vapor molecules and then push the liquid through the tube at speeds of a car on a highway. The narrow liquid stream creates a sparse vapor cloud, with water molecules spaced far enough apart that they and the reactant gases interact, at most, weakly. Experimentalists, however, confront a host of challenges: nozzle clogging, unstable jetting, searching for vacuum-compatible solutions, measuring low signal levels, and teasing out artifacts because the slender jet is the smallest surface in the vacuum chamber. In this Account, we describe lessons that we are learning as we explore gases (DCl, (HCOOH)₂, N_2O_5) reacting with water molecules and solute ions in the near-interfacial region of these fast-flowing aqueous microjets.

KEY REFERENCES

- Lancaster, D. K.; Johnson, A. M.; Burden, D. K.; Wiens, J. P.; Nathanson, G. M. Inert Gas Scattering from Liquid Hydrocarbon Microjets. J. Phys. Chem. Lett. 2013, 4, 3045–3049. This study demonstrates that it is possible to observe the scattering of gases from a liquid microjet with a diameter thinner than a strand of hair.
- Faust, J. A.; Sobyra, T. B.; Nathanson, G. M. Gas-Microjet Reactive Scattering: Collisions of HCl and DCl with Cool Salty Water. J. Phys. Chem. Lett. 2016, 7, 730—735. DCl and HCl scattering from a 7 M LiBr/H₂O microjet at 238 K showed no evidence for sub-microsecond interfacial DCl → HCl exchange, a pathway that is prominently observed in salty glycerol at room temperature.
- Sobyra, T. B.; Melvin, M. P.; Nathanson, G. M. Liquid Microjet Measurements of the Entry of Organic Acids and Bases into Salty Water. J. Phys. Chem. C 2017, 121, 20911–20924.³ Gas uptake probabilities of weak acids

- and bases into salty water microjets are measured by adapting the King and Wells reflectivity method. Despite their strong intramolecular hydrogen bonds, formic acid dimers are observed to adsorb and dissociate on almost every collision.
- Sobyra, T. B.; Pliszka, H.; Bertram, T. H.; Nathanson, G. M. Production of Br₂ from N₂O₅ and Br⁻ in Salty and Surfactant-Coated Water Microjets. J. Phys. Chem. A 2019, 123, 8942–8953. This is our first study of a gasmicrojet reaction in which the reaction product is observed in the gas phase. Both neutral and cationic surfactants

Received: September 6, 2022



Accounts of Chemical Research pubs.acs.org/accounts Article

reduce the measured Br2 product signal but for different

INTRODUCTION

The intermixing of gases and liquid water pervades our daily lives. The scale of these processes can be enormous: each year, about 10¹⁹ moles of water evaporate from oceans, 10¹⁴ moles of CO₂ and O₂ move across the alveoli in our lungs (10⁴ moles per person!), and 10¹² moles of Cl₂ are used to disinfect water. These examples highlight the evaporation, solvation, and reaction pathways that can be explored using gas-microjet scattering experiments. A chief advantage of studies in vacuum is the suppression of gas-vapor collisions that distort the trajectories of incoming and outgoing molecules, enabling investigators to focus on the gas-liquid interactions themselves using vacuum-based analytical techniques.

Liquids can be prepared in myriad ways for scattering experiments. Our own choices, inspired by Hickman, Fenn, 8 Olander, Siegbahn, on and Faubel, 5,11,12 are illustrated in Figure 1. Static crucibles may be used for reactive liquids with low vapor pressures ($<10^{-7}$ Torr in our case), such as molten metals and hydroxide and carbonate salts, whose surfaces can

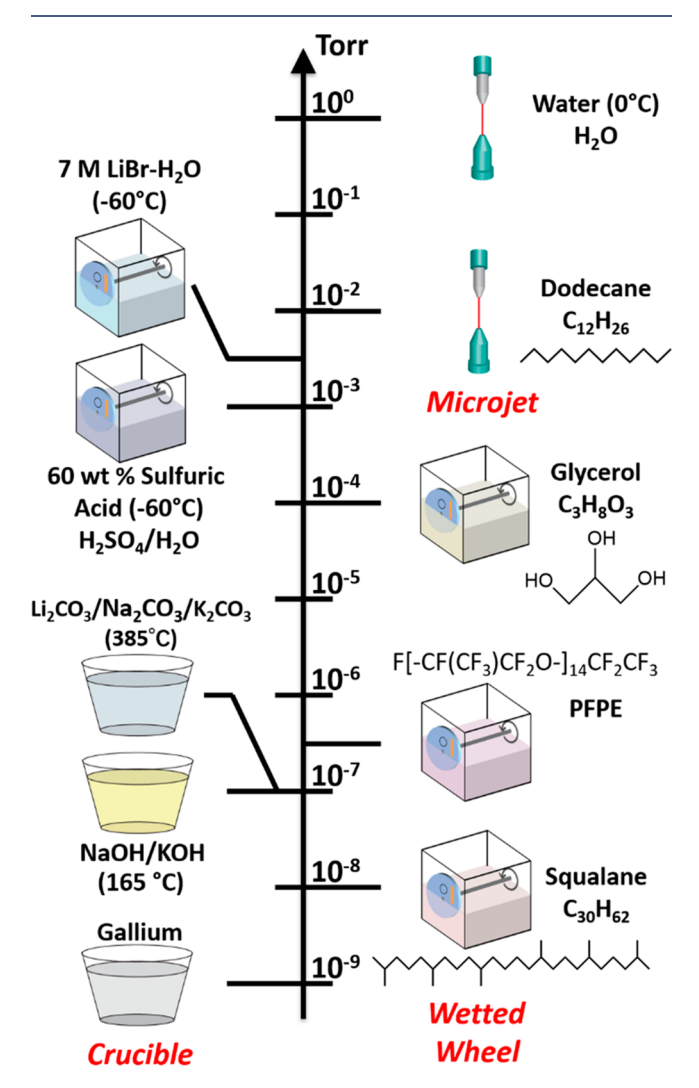


Figure 1. Three methods to prepare liquids in vacuum. The use of a crucible, wetted wheel, or microjet depends on liquid vapor pressure and reactivity.

be cleaned by ion sputtering. 13 Low vapor pressure molecular liquids ($<10^{-2}$ Torr), including long-chain hydrocarbons, pure and salty glycerol, dilute and concentrated sulfuric acid, and even cold salty water, can be interrogated by creating continuously renewed liquid films on a rotating vertical wheel half immersed in the liquid. 6,14,15 A growing community of scientists employs liquid microjets to access pure water and aqueous mixtures of all kinds in the Torr vapor pressure range (see articles in this special issue). These cylindrical jets can also be used to investigate liquid ammonia 16 and organic liquids, 17,18 including kerosene fuels. 19 Fascinating alternative approaches include tiny holes drilled in a microfluidic channel²⁰ and flat jets^{21'} for gas-dodecane scattering²² and liquid-liquid reactions (at atmospheric pressure).²³

Gas-microjet scattering methods may be used to interrogate interfacial interactions and reactions, often building on studies of gas—solid surface dynamics^{24,25} and gas—liquid kinetics.^{26,27} Microjet experiments span measurements of reaction probabilities and solvation times, collisional energy transfer involving translational and internal motions, ^{28,29} and the observation of intermediates and final products escaping into the gas phase after interfacial and bulk phase reactions. 18 These investigations help build atomic-scale pictures of adsorption and solvation and the mechanisms and energetics of reactants converting into products.

Our group has used microjets of pure and salty water and hydrocarbon fuels to explore collisions of inert and reactive gases using velocity-resolved mass spectrometry. Examples of our nonreactive studies include the startling super-Maxwellian evaporation of helium from aqueous 30,310 and hydrocarbon liquids¹⁹ and the ability of organic molecules with acidic or basic functional groups (carboxylic acids and amines) to dissolve into water on almost every collision.³ This Account focuses on the lessons that we are learning in carrying out gasmicrojet reactive scattering. We begin with guidelines from prior research on microjets, followed by lessons from our own experiences, and conclude with lessons that we hope to learn. Our reactive scattering studies encompass the "irreversible" uptake of strong acids (HCl), hydrogen bond breaking in collisions of formic acid dimers with salty water,³ the oxidation-reduction reaction of N2O5 with Br to produce gaseous Br₂,⁴ and our current studies of reactions of nearinterfacial solvated electrons.

Our microjet scattering apparatus is shown in Figure 2. An inert gas at 2-6 atm is used to pressurize the liquid, which is pushed through two filters before emerging from a 17 μ m radius glass nozzle traveling at 20-30 m/s. Liquid nitrogen cooled panels trap much of the evaporating water and condensable reactants or products, accompanied by a baffled diffusion pump that evacuates the noncondensable gases. The liquid stream is collected in a glass bulb that is cooled to -70°C to reduce evaporation. A small fraction of the scattered reagent and evaporating product molecules pass through three apertures in order to limit observation to molecules emitted over a 3 mm length of the jet. To record their speed distributions, these molecules are chopped by a time-of-flight (TOF) wheel into \sim 50 μ s packets. The molecules then travel 20 cm before being detected by a differentially pumped electron-impact mass spectrometer. The microjet nozzle may be moved vertically and horizontally to optimize the scattering signal and test for artifacts by moving the jet through the collision zone. Each experiment requires up to one liter of liquid. After the experiment is complete and the chamber is

Accounts of Chemical Research pubs.acs.org/accounts Article

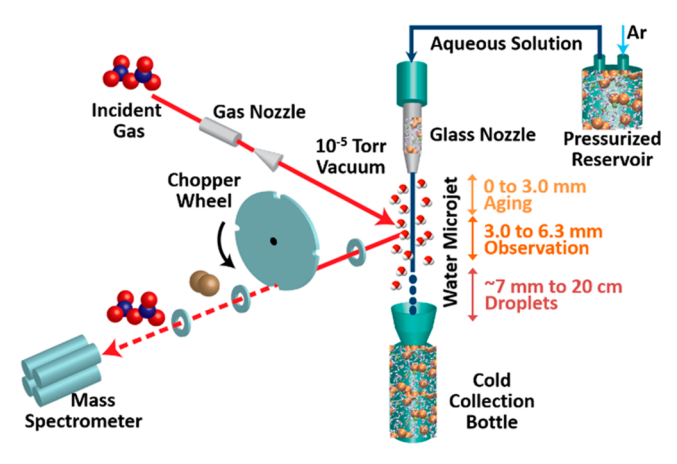


Figure 2. A gas—microjet scattering setup. Argon gas pressurizes the reservoir containing a salty solution (LiBr/H₂O) and pushes it out of the glass nozzle as a thin liquid stream, where it intersects the gas beam. The jet evolves into droplets and is collected in a cold bottle. The incident gas (N₂O₅) passes through the sparse water vapor cloud to reach the jet surface and scatter, dissolve, and evaporate or react with Br $^-$ ions or H₂O in the near-interfacial region. The exiting N₂O₅ and Br₂ are chopped into short-time packets and detected by the mass spectrometer. Adapted with permission from ref 4. Copyright 2019 American Chemical Society.

vented, we switch to a pure water jet to suppress clogging due to salt precipitation.

■ LESSONS FROM THE LITERATURE

The key insight governing microjets in vacuum was articulated in 1988 by Manfred Faubel, 5,11 who observed that the radius of a cylindrical liquid jet must be several times smaller than the vapor mean free path in order to suppress collisions in the vapor cloud surrounding the jet. In this way, most incoming and outgoing molecules pass freely through the vapor region. For a cylinder of length $L_{\rm jet}$ the number (or probability) of collisions, $N_{\rm coll}$ between the gas and vapor molecules can be gauged by counting the mean free paths, λ , over the distance, R, that the molecules travel before passing through an aperture: 6,32

$$N_{\text{coll}} = \int_{r_{\text{jet}}}^{R} \frac{dr}{\lambda(r)} \approx \frac{r_{\text{jet}}}{\lambda_{0}} \ln \left(\frac{R}{r_{\text{jet}}} \frac{L_{\text{jet}} + \sqrt{r_{\text{jet}}^{2} + L_{\text{jet}}^{2}}}{r_{\text{jet}} + \sqrt{R^{2} + L_{\text{jet}}^{2}}} \right)$$
(1)

where $\lambda_0 \approx 1/(\sigma n_{\rm vap}/2)$ and σ is the gas—vapor collision cross section. The equilibrium vapor number density $n_{\rm vap} = P_{\rm vap}/RT_{\rm jet}$ is divided by 2 because the vacuum pumps prevent recondensation of evaporating water molecules onto the jet, thereby cutting the number density in half. In practice, the aperture distance R is much larger than $r_{\rm jet}$ and $L_{\rm jet}$ and eq 1 simplifies to

$$N_{\rm coll} pprox rac{r_{
m jet}}{\lambda_0} \ln \left(rac{2L_{
m jet}}{r_{
m jet}}
ight) \propto P_{
m vap} \sigma r_{
m jet} \ln \left(rac{2L_{
m jet}}{r_{
m jet}}
ight)$$
 (2)

We find that eqs 1 and 2 are most useful for the guidance they provide in choosing the experimental and property variables $r_{\rm jet}$, $P_{\rm vap}$, and σ . The equations indicate that $N_{\rm coll}$ increases linearly with $P_{\rm vap}$ and σ and slightly less than linearly with $r_{\rm jet}$. A key uncertainty is the value of σ , which may vary from only ~ 30 Å² for hard sphere collisions among water molecules

(calculated from the liquid water density) to hundreds of Å² for long-range energy transfer. As an example, eq 1 predicts that $N_{\rm coll}$ is about 0.3 for water evaporation for typical parameters in our experiments of $\sigma=30$ Å², $r_{\rm jet}=17~\mu{\rm m}$, R=5 cm, $L_{\rm jet}=7~{\rm mm}$ (equal to the breakup length calculated below), and $P_{\rm vap}=0.5$ Torr for 7 M LiBr at 253 K (versus 24 Torr for pure water at 298 K). The fraction of evaporating water molecules that avoid gas-phase collisions, e^{$-N_{\rm coll}$}), is about 70% (see ref 29 for a deeper discussion), and evaporation is mildly supersonic.⁴ For these parameters, the collision probability reaches half its value at $R=0.5~{\rm mm}$ (15 jet diameters) from the surface.

The apparatus in Figure 2 is designed to monitor a 3 mm length of the 17 μ m radius jet exposed to the incident gas beam. The collision area is 0.08 mm² or 100 times smaller than the monitored area of a static sample or coated wheel (Figure 1). While the spectra shown here involve several hours of signal averaging (some at low signal-to-noise), the experimentalist must also be attentive to eliminating spurious signals (such as scattering from the nozzle tip) and avoiding clogged nozzles while hunting down product signals. Microjet experiments require patience!

The effects of large $N_{\rm coll}$ are at least twofold. The distributions of speeds, directions, and quantum states of the exiting molecules narrow as the molecules collide with each other and undergo adiabatic expansion. This narrowing can often be tolerated if the primary focus is searching for reaction products rather than investigating energy transfer. More pernicious is the gas—vapor scattering that reduces the number of incoming molecules that reach the jet, thereby lowering the scattering signal. The choice of jet radius is a compromise that balances signal quality and strength.

Two other phenomena should also be considered before starting experiments: evaporative cooling of the jet and the breakup of the cylindrical jet into droplets. Formulas have been developed for the extent of cooling, ΔT , and breakup length, L_{breakup} , (being careful to use SI units throughout):^{6,11}

$$\Delta T \approx \left(\frac{P_{\text{vap}}}{r_{\text{jet}}}\right) \left(\frac{z}{\nu_{\text{jet}}}\right) \frac{\Delta H_{\text{vap}}}{C_{\text{p}}\rho} \sqrt{\frac{32m_{\text{gas}}}{\pi RT}}$$
(3)

and

$$L_{\text{breakup}} \approx d_{\text{jet}} \sqrt{\frac{d_{\text{jet}} v_{\text{jet}}^2 \rho}{\gamma}} \left(1 + 3 \frac{\eta}{\sqrt{\rho \gamma d_{\text{jet}}}} \right)$$

$$\left(7.68 - 2.66 \frac{\eta}{\sqrt{\rho \gamma d_{\text{jet}}}} \right)$$
(4)

where z is the distance along the jet, $v_{\rm jet}$ is the jet speed, ρ is the mass density, η is the viscosity, and γ is the surface tension. As expected, evaporative cooling increases with vapor pressure and the time over which molecules evaporate $(z/v_{\rm jet})$. This cooling also varies inversely with jet radius because evaporation increases with jet area while cooling the jet volume, whose ratio is $2/r_{\rm jet}$. Narrow jets of high vapor pressure liquids therefore cool extensively, eventually freezing if the liquid does not supercool. The liquid temperature range can be extended by adding salts such as LiBr or LiCl, with eutectic temperatures near 200 K. These salts also reduce the vapor pressure (by half for a 7 M LiBr solution at 253 K). We monitor the jet temperature, $T_{\rm liq}$, in the interaction zone by pressurizing the

liquid reservoir with argon and then fitting the measured speed distribution of evaporating Ar atoms with a Maxwell–Boltzmann distribution at $T_{\rm liq}$. This "argon thermometry" shows that a 17 μ m radius jet of 7 M LiBr/H₂O moving at 28 m/s cools from 273 to 253 K over the ~5 mm distance from the nozzle tip to the middle of the interaction zone.³

The distance at which the cylindrical jet breaks apart into droplets depends on how quickly surface tension forces pinch off the cylinder. Equation 4 shows that the breakup length increases with jet diameter, jet speed, and solution viscosity and decreases with surface tension. The effects can be dramatic: the high surface tension (78 mN/m) and low viscosity (5 cP) of supercooled water at 253 K emerging from a 5 μ m radius at 20 m/s jet cause it to break up in <1 mm, while squalane, a lower surface tension (29 mN/m) and more viscous (32 cP) liquid at 298 K persists as a cylinder for 20 mm after emerging from a 50 μ m radius nozzle.

A key consequence of eq 4 is that the jet must move quickly, often near 30 m/s, to stay as a cylinder in the interaction region (droplets are less desirable because they scatter gas molecules more broadly). This fast-moving jet limits the exposure and observation time of the 3 mm interaction zone to just 10⁻⁴ s. Gas-liquid reactions and product evaporation must occur within this short time to monitor these processes. This 10⁻⁴ s constraint is much more severe than the time window of the rotating coated wheel, which can probe processes over seconds.6

One further relation provides guidance in estimating how long gas molecules will dissolve in solution before evaporating. A characteristic solvation time, τ , is given by $^{33-35}$

$$\tau = D \left(\frac{4HRT}{\alpha \langle v \rangle} \right)^2 \tag{5}$$

where D is the diffusion coefficient of the gas molecule in the liquid, H is its solubility in M/atm (which may include reversible reaction), ³⁶ $\langle v \rangle$ is its mean speed $(8RT/\pi m_{\rm gas})^{1/2}$, and α is the fraction of impinging gas molecules that enter the solution. This entry probability is generally close to one except for very weakly interacting gases. Inert or weakly polarizable, non-protic gases typically have low solubilities and residence times much shorter than 10^{-4} seconds and will fully evaporate, while the lifetime of hydrogen bonding and acidic gases (ethanol, carboxylic acids, HCl) can greatly exceed 10⁻⁴ s and mostly remain in solution, particularly at colder temperatures.

■ LESSONS WE HAVE LEARNED

Armed with these insights, 5,11,37,38 we started using microjets for gas-liquid scattering experiments involving water and volatile organic liquids. Along the way, we learned several lessons that guide us in designing experiments:

- Choose the largest jet diameter consistent with experimental demands to achieve the highest signal and minimize chances of nozzle clogging.
- Choose solutions whose temperature (and therefore vapor pressure) can be varied in order to investigate the effects of collisions within the vapor cloud surrounding the jet. Studies at higher temperature often benefit from initial studies at lower temperature.
- Choose solutions that become slushy in a cold bath rather than freeze. Frozen solutions may form icicles that quickly travel from the cold bath back to the nozzle tip.

We find that LiBr and LiCl solutions form slushes in an ethanol/dry ice bath at -70 °C.

- To minimize false signals, choose gaseous reagents and products that freeze or react on cold baffles (near liquid nitrogen temperature) placed near the jet. These surfaces are continuously coated with water and can react with acids and oxidants such as HCl and N₂O₅. Be aware of reagent gases (such as sodium atoms) that react on ice surfaces and generate the same product, H2, that is created in a water microjet.
- Salt solutions should be filtered to remove insoluble matter, and surface tensions should be measured to check for surfactant impurities. We avoid toxic liquids because of handling and evaporation. Viscous solutions may require backing pressures high enough that they can only safely be delivered by a liquid pump rather than a gas tank (for a fixed flow rate, the backing pressure increases linearly with η and inversely as r_{iet}^{4}). Otherwise, the sky is the limit: microjets have been made of 8 M HNO_3 , 39 13 M H_2SO_4 , 40 and 3 M NaOH, 19 jet fuel, 19 and nanoparticle-containing sol-
- Estimate collision probabilities (eq 1), evaporative cooling rates (eq 3), breakup lengths (eq 4), and solvation times (eq 5) to guide the generation and positioning of the jet and choice of solutions. 6,11,33
- The net uptake of a gas into a liquid can be measured by comparing the flux of gas reflected from the microjet to the flux of gas reflected from an inert surface (such as the glass nozzle). We find it challenging to measure nonreactive or reactive uptake probabilities smaller than a few percent.^{3,4} When uptake is reversible and the solvation time τ (eq 4) is much greater than the observation time $(10^{-4} \text{ s in our experiments})$, the net uptake approaches the initial solvation probability α . In the opposite extreme, dissolved gas evaporates during the observation time and the net uptake approaches zero. The time dependence of this reversible solvation may potentially be extracted by varying the jet speed and therefore the observation time, as is readily done with coated wheels.44
- The speed distribution of evaporating argon atoms may be used to measure the temperature of the jet in the collision zone. 2,19 SF $_6$ scattering may be used, in conjunction with benchtop surface tension measurements, to determine surface concentrations of surfac-
- We greatly benefited from spending time in established laboratories watching how microjet experiments fail as well as succeed. The microjet community eagerly supports each other. Ask questions!

LESSONS IN THE CONTEXT OF OUR **EXPERIMENTS**

In the following paragraphs, we summarize our reactive scattering experiments with respect to the lessons listed above and then mention new experiments and lessons we hope to learn.

Dissociation of Strong Acids in Salty Water^{2,43}

We began gas-microjet reactive scattering by investigating collisions of the strong acids HCl and DCl with a 35 μ m diameter jet of 7 M LiBr/H₂O at 238 K, whose vapor pressure

Accounts of Chemical Research pubs.acs.org/accounts Article

is 0.1 Torr. Our study was motivated by the observation that impinging DCl molecules undergo sub-microsecond nearinterfacial DCl -> HCl exchange with liquid glycerol, HOCH₂CH(OH)CH₂OH, a strongly hydrogen bonding and viscous liquid with a vapor pressure of 10⁻⁴ Torr at 298 K.⁴³ This "ultrafast" DCl production was attributed to $D^+ \rightarrow H^+$ exchange with neighboring near-interfacial glycerol molecules, followed by immediate H⁺ association with the original Cl⁻ before the ions migrate away from each other. The addition of up to 5 M NaI or 3 M CaI₂ enhances this rapid exchange channel from 3% to as high as 15%. This enhancement may arise because the Ca2+, Na+, and I- ions can block the Grotthuss proton relay that rapidly transports H⁺ always from the collision zone, instead localizing the H⁺ and Cl⁻ ions near each other to create HCl that then escapes. We were eager to learn if this rapid DCl → HCl exchange exists in salty water as well, which could be tested in a microjet (we failed earlier to observe this exchange in 6 M LiCl/H2O at 212 K and 0.005 Torr vapor pressure using a coated wheel¹⁵).

Figure 3b depicts DCl scattering from a 7 M LiBr/ H_2O jet at 238 K, or 26 K higher temperature and 20 times higher vapor pressure than with the coated wheel. For reference, panel a illustrates scattering of HCl from a strand of hair that is 55 μ m thick: HCl scatters directly (high speeds and short arrival

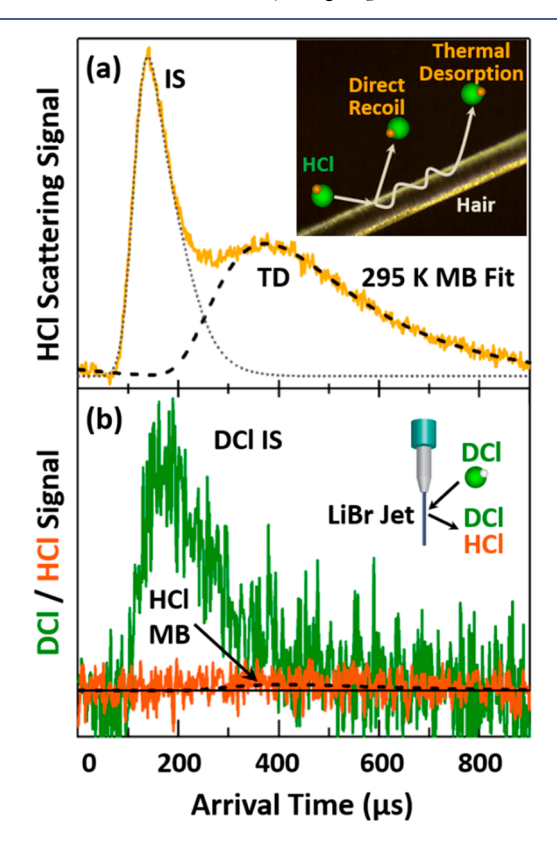


Figure 3. (a) Time-of-flight spectra of HCl following collisions with a 55 μ m diameter strand of hair. The fast (dotted line) and slow (dashed line) channels originate from inelastic scattering (IS) and trapping desorption (TD). The dashed line is a Maxwellian–Boltzmann (MB) distribution at the 295 K temperature of the hair. (b) TOF spectra of HCl (orange) and DCl (green) following collisions of DCl with a 35 μ m diameter jet of 7 M LiBr/H₂O at 238 K (0.1 Torr vapor pressure). There is almost no thermal desorption of DCl or HCl, which instead remain as dissolved D⁺, H⁺, and Cl⁻. Adapted from ref 2. Copyright 2016 American Chemical Society.

times: inelastic scattering, IS) and by dissipating its excess energy and becoming momentarily trapped at the surface and then desorbing (low speeds and long arrival times: trapping desorption, TD). These two outcomes are often observed in high-energy scattering, with distinct times of arrival that allow the two pathways to be separated. Panel b shows DCl scattering at high collision energy from the salty solution. The absence of a DCl or HCl TD channel indicates that essentially all thermally accommodated DCl molecules enter the water jet and do not reemerge, either as unreacted DCl or as protonexchanged HCl. There is thus no evidence for the rapid DCl → HCl exchange channel that is so evident in DCl scattering from liquid glycerol, perhaps because the full three-dimensional hydrogen bonding network of H₂O and its low viscosity can always shuttle D⁺/H⁺ away from the reaction zone even in high salt concentrations.

We learned three valuable lessons from this study. First, it is possible to monitor gas-liquid reactions from a liquid target that is thinner than a strand of hair. Second, we did not observe either fast or slow recombination of H⁺ and Cl⁻ to produce evaporating HCl. The absence of even slow HCl evaporation arises from the short 10⁻⁴ s observation time and the much greater solubility of H⁺ and Cl⁻ in salty water at 238 K than in salty glycerol at 293 K (where slow H⁺ + Cl⁻ recombination and HCl evaporation was observed).44 These observations led to a third lesson: fascinating interfacial and bulk-phase phenomena can be observed using liquids other than water! We find that reactions in liquids like glycerol can stimulate questions about reactions in water that might not otherwise be asked. We hope to repeat the microjet experiments near 273 K to learn if higher temperatures allow rapid near-interfacial D \rightarrow H exchange and desorption of HCl before it dissociates into separately solvated ions.

Hydrogen Bond Dissociation in Formic Acid Dimer³

We next examined the way in which intramolecular hydrogen bonds are broken upon adsorption of formic acid dimers to two salty water solutions, 7 M LiBr/H₂O and 3 M K₂SO₃/ H₂O, at 253 K. The formic acid dimer is shown in Figure 4a. The two intramolecular hydrogen bonds tie up the protic H atoms and one lone pair on each carbonyl oxygen. Can these hydrogen bonds render the dimer hydrophobic, such that the dimer can adsorb on the surface of water and evaporate before it falls apart in the near-interfacial region? Panels b-d demonstrate that the answer is no: there is no evidence for evaporation of the dimer when delivered to the surface at high or low collision energies. We measure an escape probability of the thermally accommodated dimer to be less than 1%, and therefore a dimer dissociation probability exceeding 99%. Molecular dynamics simulations indicate that the uncapped hydrogen bonding sites in (HCOOH), readily form hydrogen bonds to surface H₂O.⁴⁵ As illustrated in Figure 4a, the hydroxyl C-O(H)···HOH and carbonyl C=O···HOH sites in particular lead to the opening of the dimer bond and solvation of the monomer. Intriguingly, the absence of dimer desorption following dimer scattering is distinct from the observation by Faubel and Kisters that dissolved formic acid generates highly energetic dimers that evaporate from solution. 46 These dimers may be formed just below the surface and are jettisoned into the gas phase before they have a chance to dissociate.

We again learned valuable lessons from this study. It is possible to measure absolute entry probabilities, in this case, by comparing the flux of formic acid dimers reflecting from the jet Accounts of Chemical Research pubs.acs.org/accounts Article

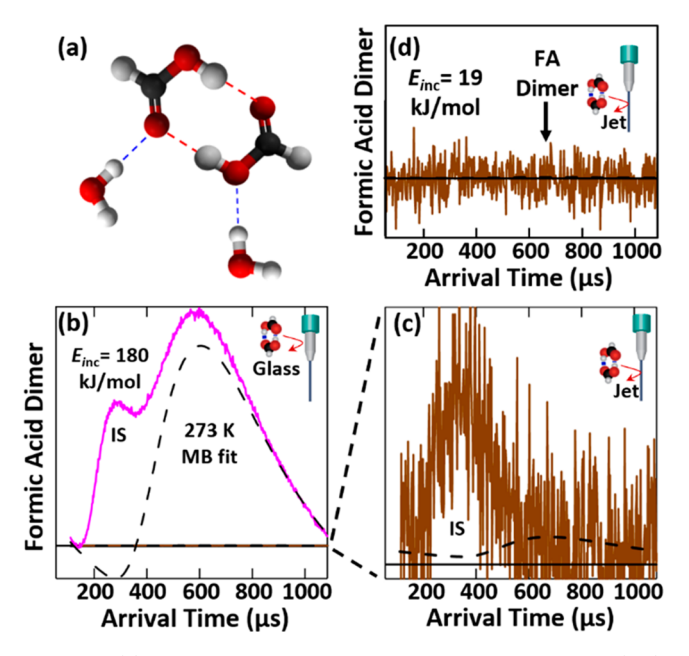


Figure 4. (a) Unfilled hydrogen bonding sites in the formic acid (FA) dimer. See ref 43 for more information. (b, c) Scattering of high energy ($E_{\rm inc}$) FA dimer (b) from the glass nozzle and (c) from a 7 M LiBr/H₂O jet at 253 K, enlarged 90-fold. (d) Scattering of low energy FA dimer from the same jet. The dashed lines are Maxwellian—Boltzmann (MB) distributions at the nozzle and jet temperatures. The arrow indicates the peak position of the MB fit. We do not observe dimer or monomer desorption from the jet. Adapted from ref 3. Copyright 2017 American Chemical Society.

with the flux of dimers reflecting from the glass nozzle. Additionally, the experiments were performed with both LiBr and $\rm K_2SO_3$ salts to determine if ion identity altered the results (it did not). $\rm K_2SO_3$ was chosen because doubly charged $\rm SO_3^{\ 2-}$ should be less populated than Br $^-$ in the interfacial region, thereby testing the role of salt ions in the dimer breakup.

We also learned how challenging it can be to create salty solutions that do not clog the nozzle (K_2SO_3 is more fickle to use than LiBr or LiCl), that do not freeze in the reservoir, that are high purity, and that are free of surfactants. The literature is replete with single salt + water phase diagrams, but multicomponent salt + water data are scarcer and instead require benchtop measurements. We recently found a solution containing the nitrate anion, 5 M LiNO $_3$ + 3 M CaCl $_2$, that is slushy and does not form icicles at $-70\,^{\circ}$ C, but its high viscosity at 243 K requires 17 atm backing pressure to form a microjet.

Observing the Product of a Chemical Reaction⁴

The two experiments described above provided null results: DCl and formic acid dimer both disappeared into solution without generating observable products. Can we find a reaction whose gas-phase products can be observed and controlled? The answer turned out to be an important atmospheric reaction suggested by our colleague Timothy Bertram: the nighttime oxidation of Br $^-$ by N_2O_5 : $N_2O_5(g) + 2Br^-(aq) \rightarrow$ $Br_2(g) + NO_2^-(aq) + NO_3^-(aq)$. This aerosol-mediated reaction generates gaseous Br2, which then photolyzes to produce reactive Br atoms in the atmosphere. Figure 5a illustrates one possible mechanism involving a BrNO₂ intermediate formed from Br and N2O5. This intermediate is rapidly attacked by Br - to produce Br2, which can react reversibly with another Br to form Br₃-. Figure 5b indeed shows product Br₂ evaporating from a 5 M LiBr solution at 263 K and a 7 M LiBr solution at 240 K. The non-Maxwellian distribution at 263 K is likely due to collisions of Br₂ with evaporating H₂O in the vapor cloud, generating a mild supersonic expansion that is largely suppressed in the lower density cloud at 240 K.

Now that product Br_2 can be detected, we can ask whether Br_2 production changes in the presence of a soluble surfactant that might block N_2O_5 entry and access to near-interfacial Br^- ions. We find that the addition of 0.02 M 1-butanol creates

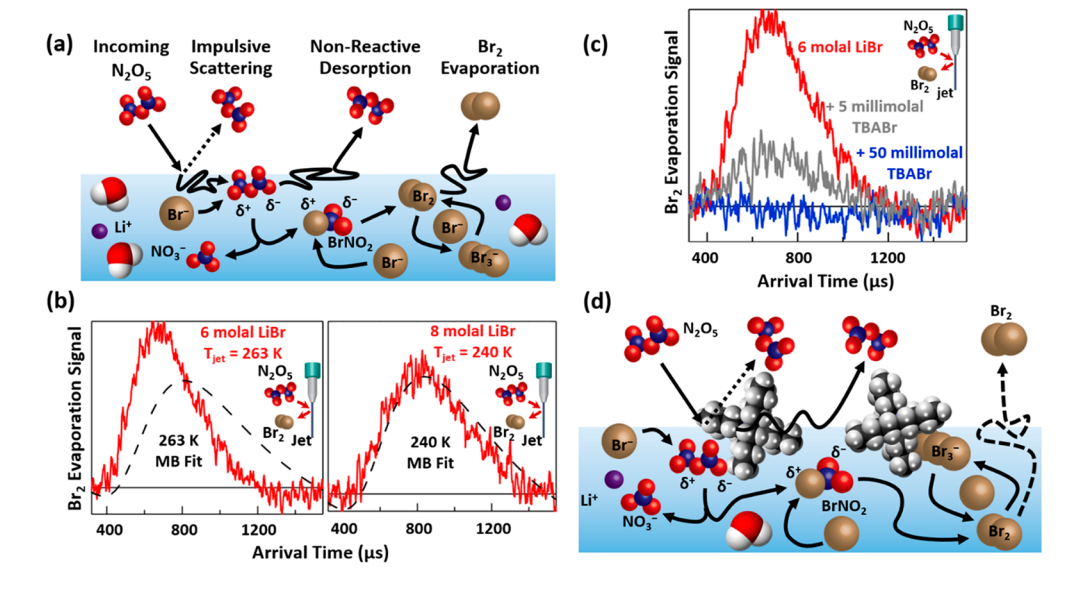


Figure 5. (a) Scattering pathways for the reaction $N_2O_5(g) + 2Br^-(aq) \rightarrow Br_2(g) + NO_2^-(aq) + NO_3^-(aq)$. (b) Evaporation of Br_2 following reactive uptake of N_2O_5 into 5 M LiBr/H₂O at 263 K (left) and 7 M LiBr/H₂O at 240 K (right). The dash lines are Maxwellian–Boltzmann (MB) distributions at the jet temperatures. (c) Evaporation of Br_2 following uptake of N_2O_5 into 5 M LiBr/H₂O with added 0 mM (red), 6 mM (gray), and 60 mM (blue) tetrabutylammonium bromide (TBABr). (d) Added TBABr traps Br_2 as Br_3^- and delays its evaporation. Adapted from ref 4. Copyright 2019 American Chemical Society.

40% of a compact monolayer and reduces the Br_2 signal by 35%, indicating that neutral surfactants can impede reaction. The effects of adding a cationic surfactant, tetrabutylammonium bromide (TBABr), were much more dramatic. Figure 5c shows that the addition of 0.006 M TBABr lowered the Br_2 signal by 85% and 0.06 M TBABr eliminated the signal, even when the surface coverage is only 60% of a compact monolayer.

Why is the Br₂ signal reduced to zero when entry should not be fully blocked? The reason, we think, is a chemical one, shown in Figure 5d: the Br₃ intermediate forms an extraordinarily strong complex with the TBA+ cation. Thus, while Br_2 is formed, it cannot escape within the 10^{-4} s observation window because it is tied up as TBA+/Br₃-. Again, prior studies in glycerol using a rotating wheel coated with a 3 M NaBr solution provided the rationale. 48 The fast, 30 μ s evaporation of Br₂ from NaBr/glycerol exceeds 0.1 s upon adding 0.03 M of a slightly larger cation, tetrahexylammonium, confirming that Br₂ is indeed produced but its evaporation is delayed by complexation between Br₃⁻ and the organic cation. Intriguingly, these glycerol studies demonstrate that alkylammonium bromides actually accelerate gas-liquid reactions by enhancing Br⁻ concentrations in the interfacial region.⁴⁸ X-ray photoelectron and kinetics experiments demonstrate this acceleration in water as well.⁴⁹

The additional lessons we learned are twofold. First, it is possible to observe a gas-phase product, in this case Br_2 , in a gas-microjet reaction. The solubility and residence time of the product should be carefully assessed: it must evaporate within the short observation window to be detected. Second, we found that the interfacial concentrations of surfactants in the jet can be measured within the observation window by highenergy SF_6 scattering. In particular, changes in direct inelastic scattering of SF_6 from surfactant solutions track changes in surface concentration determined by benchtop surface tension measurements. It was delightful to learn that inert gases can be used to characterize the temperature (Ar evaporation 2,19) and surface composition (SF_6 scattering of microjet solutions.

■ LESSONS THAT WE HOPE TO LEARN

Our current experiments focus on reactions of interfacial solvated electrons at the surfaces of salty and surfactant-coated water. These electrons are created by exposing the microjet to gaseous sodium atoms, which ionize into Na $^{+}$ and e $^{-}$ upon entering the top few monolayers. Experiments with dissolved NO $_3^{-}$ and benzyl ammonium surfactants in water are promising so far, with gaseous NO $_2$, benzyl, and amine reaction products being identified. A key question is whether we can isolate reactions within the interfacial region by adding chemical scavengers that impede bulk-phase reactivity. One signature of near-interfacial processes is the observation of gasphase reaction intermediates (such as benzyl) that escape before reacting within solution. 50

Our long-term goal is to explore higher temperature aqueous solutions, which should be accessible with narrower jets, higher gas fluxes, and more tolerance for gas—vapor collisions. It will be intriguing to probe more complex solutions that mimic, for example, the sea surface microlayer or alveolar fluid. Such efforts will benefit from collaborations that combine scattering experiments with photoelectron and photon spectroscopies presented elsewhere in this special issue.

The appreciation of gas—liquid phenomena began in ancient times and yet is still so current, particularly in aerosol and ocean chemistry^{51,52} and in fields such as sonochemistry⁵³ and fuel combustion.⁵⁴ We are driven by the desire to explore collisions and reactions between gases and liquids and imagine them at the atomic scale. Microjets are taking us a big step further

AUTHOR INFORMATION

Corresponding Author

Gilbert M. Nathanson — Department of Chemistry, University of Wisconsin—Madison, Madison, Wisconsin 53706, United States; orcid.org/0000-0002-6921-6841; Email: nathanson@chem.wisc.edu

Author

Xiao-Fei Gao — Department of Chemistry, University of Wisconsin—Madison, Madison, Wisconsin 53706, United States; ⊚ orcid.org/0000-0002-9792-6218

Complete contact information is available at: https://pubs.acs.org/10.1021/acs.accounts.2c00602

Note

The authors declare no competing financial interest.

Biographies

Xiao-Fei Gao received her Ph.D. degree from the University of Science and Technology of China under the direction of Shan Xi Tian. She is currently a postdoctoral researcher with Gilbert Nathanson and Timothy Bertram at the University of Wisconsin—Madison. Her research interests focus on the chemical reactions at gas—liquid interfaces, particularly involving solvated electrons and atmospheric gases with sea spray mimics.

Gilbert Nathanson has been a faculty member at the University of Wisconsin—Madison since 1988, following much appreciated training with his graduate and postdoctoral mentors Gary McClelland and Yuan Lee. In addition to directing research in gas—liquid scattering experiments, Gil likes to teach general chemistry and coordinate hands-on soap bubble activities for children of all ages.

ACKNOWLEDGMENTS

This research has been supported by the Air Force Office of Scientific Research, the Chemistry Division of the National Science Foundation (CHE-1900045), and the NSF Center for Aerosol Impacts on Chemistry of the Environment (CHE-1801971). It is a pleasure to thank Alexis Johnson, Diane Lancaster, Jennifer Faust, Christine Hahn, Tom Sobyra, and David Hood for their many hours of creative and dogged efforts to make the microjet experiments work. We also thank Kevin Wilson, Rich Saykally, Ron Cohen, Dan Neumark, John Hemminger, David Nesbitt, and Shan Xi Tian and their students for sharing their time and expertise in the intricacies of microjets and the microjet magician Manfred Faubel for sharing his insights and enthusiasm.

REFERENCES

- (1) Lancaster, D. K.; Johnson, A. M.; Burden, D. K.; Wiens, J. P.; Nathanson, G. M. Inert Gas Scattering from Liquid Hydrocarbon Microjets. *J. Phys. Chem. Lett.* **2013**, *4*, 3045–3049.
- (2) Faust, J. A.; Sobyra, T. B.; Nathanson, G. M. Gas-Microjet Reactive Scattering: Collisions of HCl and DCl with Cool Salty Water. *J. Phys. Chem. Lett.* **2016**, *7*, 730–735.

- (3) Sobyra, T. B.; Melvin, M. P.; Nathanson, G. M. Liquid Microjet Measurements of the Entry of Organic Acids and Bases into Salty Water. J. Phys. Chem. C 2017, 121, 20911–20924.
- (4) Sobyra, T. B.; Pliszka, H.; Bertram, T. H.; Nathanson, G. M. Production of Br₂ from N₂O₅ and Br⁻ in Salty and Surfactant-Coated Water Microjets. *J. Phys. Chem. A* **2019**, *123*, 8942–8953.
- (5) Faubel, M.; Schlemmer, S.; Toennies, J. P. Molecular-Beam Study of the Evaporation of Water from a Liquid Jet. *Z. Phys. D-Atoms Mol. Clusters* **1988**, *10*, 269–277.
- (6) Faust, J. A.; Nathanson, G. M. Microjets and Coated Wheels: Versatile Tools for Exploring Collisions and Reactions at Gas-Liquid Interfaces. *Chem. Soc. Rev.* **2016**, *45*, 3609–3620.
- (7) Hickman, K. C. D. Surface Behavior in the Pot Still. *Industrial & Engineering Chemistry* **1952**, 44, 1892–1902.
- (8) Lednovich, S. L.; Fenn, J. B. Absolute Evaporation Rates for Some Polar and Nonpolar Liquids. *AIChE J.* **1977**, 23, 454–459.
- (9) Balooch, M.; Siekhaus, W. J.; Olander, D. R. Reactions of Chlorine with Liquid-Metals. 1. Indium. *J. Phys. Chem.* **1984**, 88, 3521–3528.
- (10) Siegbahn, H. Electron-Spectroscopy for Chemical-Analysis of Liquids and Solutions. *J. Phys. Chem.* **1985**, *89*, 897–909.
- (11) Faubel, M. Photoelectron Spectroscopy at Liquid Surfaces. In *Photoionization and Photodetachment*; World Scientific: Singapore, 1999; Part I, pp 634–690.
- (12) Winter, B. Liquid Microjet for Photoelectron Spectroscopy. *Nucl. Instrum. Methods Phys. Res. Sect. A-Accel. Spectrom. Dect. Assoc. Equip.* **2009**, 601, 139–150.
- (13) Ronk, W. R.; Kowalski, D. V.; Manning, M.; Nathanson, G. M. Inert Gas Scattering from Molten Metals: Probing the Stiffness and Roughness of the Surfaces of Atomic Liquids. *J. Chem. Phys.* **1996**, 104, 4842–4849.
- (14) Tesa-Serrate, M. A.; Smoll, E. J.; Minton, T. K.; McKendrick, K. G. Atomic and Molecular Collisions at Liquid Surfaces. *Annu. Rev. Phys. Chem.* **2016**, *67*, 515–540.
- (15) Brastad, S. M.; Nathanson, G. M. Molecular Beam Studies of HCl Dissolution and Dissociation in Cold Salty Water. *Phys. Chem. Chem. Phys.* **2011**, *13*, 8284–8295.
- (16) Buttersack, T.; Mason, P. E.; McMullen, R. S.; Martinek, T.; Brezina, K.; Hein, D.; Ali, H.; Kolbeck, C.; Schewe, C.; Malerz, S.; Winter, B.; Seidel, R.; Marsalek, O.; Jungwirth, P.; Bradforth, S. E. Valence and Core-Level X-ray Photoelectron Spectroscopy of a Liquid Ammonia Microjet. J. Am. Chem. Soc. 2019, 141, 1838–1841.
- (17) Faubel, M.; Steiner, B.; Toennies, J. P. Photoelectron Spectroscopy of Liquid Water, Some Alcohols, and Pure Nonane in Free Micro Jets. *J. Chem. Phys.* **1997**, *106*, 9013–9031.
- (18) Li, Z. Y.; Fu, C. F.; Chen, Z. W.; Tong, T. T.; Hu, J.; Yang, J. L.; Tian, S. X. Electron-Induced Synthesis of Dimethyl Ether in the Liquid-Vapor Interface of Methanol. *J. Phys. Chem. Lett.* **2022**, *13*, 5220–5225.
- (19) Lancaster, D. K.; Johnson, A. M.; Kappes, K.; Nathanson, G. M. Probing Gas-Liquid Interfacial Dynamics by Helium Evaporation from Hydrocarbon Liquids and Jet Fuels. *J. Phys. Chem. C* **2015**, *119*, 14613–14623.
- (20) Yu, X. Y. In Vivo, and In Operando Imaging and Spectroscopy of Liquids Using Microfluidics in Vacuum. *J. Vac. Sci. Technol. A* **2020**, 38, 040804
- (21) Ekimova, M.; Quevedo, W.; Faubel, M.; Wernet, P.; Nibbering, E. T. J. A Liquid Flatjet System for Solution Phase Soft-X-Ray Spectroscopy. *Struct. Dyn.-US* **2015**, *2*, 054301.
- (22) Lee, C.; Pohl, M. N.; Ramphal, I. A.; Yang, W.; Winter, B.; Abel, B.; Neumark, D. M. Evaporation and Molecular Beam Scattering from a Flat Liquid Jet. *J. Phys. Chem. A* **2022**, *126*, 3373–3383.
- (23) Schewe, H. C.; Credidio, B.; Ghrist, A. M.; Malerz, S.; Ozga, C.; Knie, A.; Haak, H.; Meijer, G.; Winter, B.; Osterwalder, A. Imaging of Chemical Kinetics at the Water-Water Interface in a Free-Flowing Liquid Flat-Jet. J. Am. Chem. Soc. 2022, 144, 7790–7795.

- (24) Rettner, C. T.; Auerbach, D. J.; Tully, J. C.; Kleyn, A. W. Chemical Dynamics at the Gas-Surface Interface. *J. Phys. Chem.* **1996**, 100, 13021–13033.
- (25) Kolasinski, K. W. Surface Science: Foundations of Catalysis and Nanoscience; John Wiley & Sons: Chichester, 2012; Chapters 3 and 4.
- (26) Davidovits, P.; Kolb, C. E.; Williams, L. R.; Jayne, J. T.; Worsnop, D. R. Mass Accommodation and Chemical Reactions at Gas-Liquid Interfaces. *Chem. Rev.* **2006**, *106*, 1323–1354.
- (27) Willis, M. D.; Wilson, K. R. Coupled Interfacial and Bulk Kinetics Govern the Timescales of Multiphase Ozonolysis Reactions. *J. Phys. Chem. A* **2022**, *126*, 4991–5010.
- (28) Maselli, O. J.; Gascooke, J. R.; Lawrance, W. D.; Buntine, M. A. The Dynamics of Evaporation from a Liquid Surface. *Chem. Phys. Lett.* **2011**, *513*, 1–11.
- (29) Ryazanov, M.; Nesbitt, D. J. Quantum-State-Resolved Studies of Aqueous Evaporation Dynamics: NO Ejection from a Liquid Water Microjet. *J. Chem. Phys.* **2019**, *150*, 044201.
- (30) Hahn, C.; Kann, Z. R.; Faust, J. A.; Skinner, J. L.; Nathanson, G. M. Super-Maxwellian Helium Evaporation from Pure and Salty Water. J. Chem. Phys. 2016, 144, 044707.
- (31) Nathanson, G. M. When Liquid Rays Become Gas Rays: Can Evaporation Ever Be Non-Maxwellian? In Molecular Beams in Physics and Chemistry: From Otto Stern's Pioneering Exploits to Present-Day Feats; Springer International Publishing, 2021; pp 631–647.
- (32) Sadtchenko, V.; Brindza, M.; Chonde, M.; Palmore, B.; Eom, R. The Vaporization Rate of Ice at Temperatures Near Its Melting Point. *J. Chem. Phys.* **2004**, *121*, 11980–11992.
- (33) Schwartz, S. E.; Freiberg, J. E. Mass-Transport Limitation to the Rate of Reaction of Gases in Liquid Droplets: Application to Oxidation of SO_2 in Aqueous Solutions. *Atmos. Environ.* (1967) **1981**, 15 (15), 1129–1144.
- (34) Jayne, J. T.; Davidovits, P.; Worsnop, D. R.; Zahniser, M. S.; Kolb, C. E. Uptake of Sulfur Dioxide (G) by Aqueous Surfaces as a Function of Ph: the Effect of Chemical Reaction at the Interface. *J. Phys. Chem.* **1990**, *94*, 6041–6048.
- (35) Nathanson, G. M. Molecular Beam Studies of Gas-Liquid Interfaces. *Annu. Rev. Phys. Chem.* **2004**, 55, 231–255.
- (36) Sander, R. Compilation of Henry's Law Constants (Version 4.0) for Water as Solvent. *Atmos. Chem. Phys.* **2015**, *15*, 4399–4981.
- (37) Kondow, T.; Mafune, F. Structures and Dynamics of Molecules on Liquid Beam Surfaces. *Annu. Rev. Phys. Chem.* **2000**, *51*, 731.
- (38) Wilson, K. R.; Rude, B. S.; Smith, J.; Cappa, C.; Co, D. T.; Schaller, R. D.; Larsson, M.; Catalano, T.; Saykally, R. J. Investigation of Volatile Liquid Surfaces by Synchrotron X-Ray Spectroscopy of Liquid Microjets. *Rev. Sci. Instrum.* **2004**, *75*, 725–736.
- (39) Lewis, T.; Winter, B.; Stern, A. C.; Baer, M. D.; Mundy, C. J.; Tobias, D. J.; Hemminger, J. C. Does Nitric Acid Dissociate at the Aqueous Solution Surface? *J. Phys. Chem. C* **2011**, *115*, 21183–21190.
- (40) Margarella, A. M.; Perrine, K. A.; Lewis, T.; Faubel, M.; Winter, B.; Hemminger, J. C. Dissociation of Sulfuric Acid in Aqueous Solution: Determination of the Photoelectron Spectral Fingerprints of H₂SO₄, HSO₄⁻, and SO₄²⁻ in Water. *J. Phys. Chem. C* **2013**, *117*, 8131–8137.
- (41) Winter, B.; Faubel, M.; Vacha, R.; Jungwirth, P. Behavior of Hydroxide at the Water/Vapor Interface. *Chem. Phys. Lett.* **2009**, 474, 241–247.
- (42) Brown, M. A.; Seidel, R.; Thurmer, S.; Faubel, M.; Hemminger, J. C.; van Bokhoven, J. A.; Winter, B.; Sterrer, M. Electronic Structure of Sub-10 nm Colloidal Silica Nanoparticles Measured by In Situ Photoelectron Spectroscopy at the Aqueous-Solid Interface. *Phys. Chem. Chem. Phys.* **2011**, *13*, 12720–12723.
- (43) Dempsey, L. P.; Brastad, S. M.; Nathanson, G. M. Interfacial Acid Dissociation and Proton Exchange Following Collisions of DCl with Salty Glycerol and Salty Water. *J. Phys. Chem. Lett.* **2011**, *2*, 622–627.
- (44) Ringeisen, B. R.; Muenter, A. H.; Nathanson, G. M. Collisions of HCl, DCl, and HBr with Liquid Glycerol: Gas Uptake, D \rightarrow H Exchange, and Solution Thermodynamics. *J. Phys. Chem. B* **2002**, *106*, 4988–4998.

- (45) Hanninen, V.; Murdachaew, G.; Nathanson, G. M.; Gerber, R. B.; Halonen, L. Ab Initio Molecular Dynamics Studies of Formic Acid Dimer Colliding with Liquid Water. Phys. Chem. Chem. Phys. 2018, 20, 23717-23725.
- (46) Faubel, M.; Kisters, T. Non-Equilibrium Molecular Evaporation of Carboxylic-Acid Dimers. Nature 1989, 339, 527-529.
- (47) Park, S. C.; Burden, D. K.; Nathanson, G. M. Surfactant Control of Gas Transport and Reactions at the Surface of Sulfuric Acid. Acc. Chem. Res. 2009, 42, 379-387.
- (48) Faust, J. A.; Dempsey, L. P.; Nathanson, G. M. Surfactant-Promoted Reactions of Cl₂ and Br₂ with Br⁻ in Glycerol. J. Phys. Chem. B 2013, 117, 12602-12612.
- (49) Chen, S. Z.; Artiglia, L.; Orlando, F.; Edebeli, J.; Kong, X. R.; Yang, H. Y.; Boucly, A.; Corral Arroyo, P.; Prisle, N.; Ammann, M. Impact of Tetrabutylammonium on the Oxidation of Bromide by Ozone. ACS Earth Space Chem. 2021, 5, 3008-3021.
- (50) Alexander, W. A.; Wiens, J. P.; Minton, T. K.; Nathanson, G. M. Reactions of Solvated Electrons Initiated by Sodium Atom Ionization at the Vacuum-Liquid Interface. Science 2012, 335, 1072-
- (51) Cochran, R. E.; Ryder, O. S.; Grassian, V. H.; Prather, K. A. Sea Spray Aerosol: The Chemical Link between the Oceans, Atmosphere, and Climate. Acc. Chem. Res. 2017, 50, 599-604.
- (52) Novak, G. A.; Bertram, T. H. Reactive VOC Production from Photochemical and Heterogeneous Reactions Occurring at the Air-Ocean Interface. Acc. Chem. Res. 2020, 53, 1014-1023.
- (53) Suslick, K. S.; Eddingsaas, N. C.; Flannigan, D. J.; Hopkins, S. D.; Xu, H. X. The Chemical History of a Bubble. Acc. Chem. Res. **2018**, *51*, 2169–2178.
- (54) Shinjo, J.; Xia, J.; Ganippa, L. C.; Megaritis, A. Physics of Puffing and Microexplosion of Emulsion Fuel Droplets. Phys. Fluids 2014, 26, 103302.

□ Recommended by ACS

High-Pressure Scanning Tunneling Microscopy

Miquel Salmeron and Baran Eren

DECEMBER 08, 2020 CHEMICAL REVIEWS

READ **Z**

Visualizing the Gas Diffusion Induced Ignition of a Catalytic Reaction

Sebastian Pfaff, Johan Zetterberg, et al.

MAY 19, 2022 ACS CATALYSIS

READ **C**

Terahertz Vibrational Motions Mediate Gas Uptake in **Organic Clathrates**

Wei Zhang, Daniel M. Mittleman, et al.

JULY 23, 2020

CRYSTAL GROWTH & DESIGN

READ **C**

Transport-Based Modeling of Bubble Nucleation on Gas **Evolving Electrodes**

Zhengmao Lu, Jeffrey C. Grossman, et al.

DECEMBER 01, 2020

LANGMUIR

READ **'**

Get More Suggestions >